Modeling for surge control of centrifugal compresssors: comparison with experiment

Jan Tommy Gravdahl*, Frank Willems**, Bram de Jager** and Olav Egeland*

* Department of Engineering Cybernetics, Norwegian University of Science and Technology,
N-7491 Trondheim, Norway
** Faculty of Mechanical Engineering, Eindhoven University of Technology, P.O. Box 513,
5600 MB Eindhoven, The Netherlands

Abstract

A dynamic model based on the thermo- and fluid-mechanic processes taking place in a centrifugal compressor is validated. The background for this is the need for a energy based model including the rotational speed as a state in order to perform energy based active surge control. The response of the model is compared with experimental results from the Energy Technology Laboratory at Eindhoven University of Technology. Both the calculated compressor characteristic and transient responses for set point changes and in-surge response were compared to experiment with good results.

1 Introduction

In this paper a dynamic model, suitable for surge control design, of a centrifugal compression system is validated. Compressor surge is an unwanted oscillation of the mass flow, pressure rise and rotational speed. Traditionally, the solution to this problem is surge avoidance: The compressor operating point is never allowed to go closer to the stability limit (the surge line), than a prescribed surge margin. The surge margin prohibits operation at maximum pressure rise and efficiency, and it narrows the operating range of the compressor. Active surge control is an attractive alternative to surge avoidance: Measurements from one or more states is fed through a control law to an actuator, and the unstable area of the compressor map can be stabilized.

In designing the active surge control law, the control engineer is dependent on a dynamic model of the compression system. Such a model will be derived in this paper. The model includes the states: mass flow, pressure rise and rotational speed. A classical result in this field is the axial compressor model of [5], where a model for mass flow and pressure rise was presented. In [6] it was shown that the model of [5] is also applicable to centrifugal compressors. Since compressors are variable speed machines, and surge is commonly encountered during speed transients and set point changes, it is of interest to investigate the influence of speed transients on the surge dynamics, and on the compressor dynamics in general. A model describing this interaction was developed in [2], where rotational speed was included as a state in the model. This approach will also be taken here, but the modeling of the compressor pressure rise and torque will be modeled in more detail, studying the energy transfer from the impeller to the fluid, and taking account for various loss mechanisms. This results in a model and a compressor characteristic that is based on the fluid-dynamic and thermo-dynamic

processes taking place in the compressor stage, as opposed to polynomial approximations or measured characteristics that has been commonly used in the surge control literature. This modeling approach is used with energy based control design in mind. When e.g. using passivity as a design tool, it is advantageous to have correct information on how energy flows in the system. This is a approach that has proven successful in other branches of control of mechanical systems, such as robotics or vehicle control.
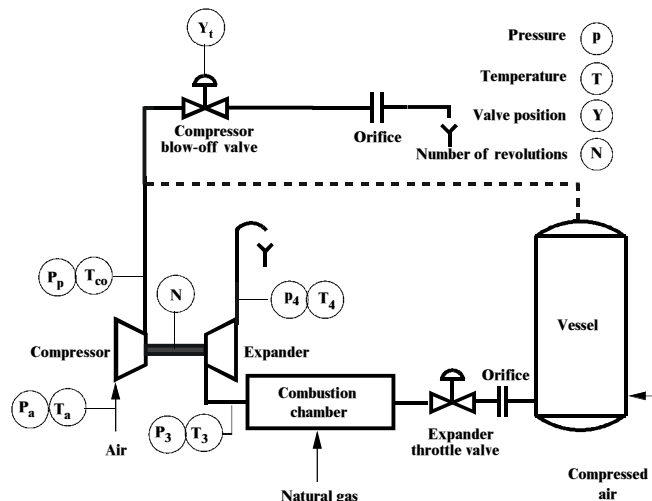
2 Experimental Set-Up

Figure 1: Scheme of experimental set up

2.1 Compression system

To study the dynamic behavior of turbomachinery, a laboratory-scale gas turbine installation was erected in the Energy Technology Laboratory of Eindhoven University of Technology. This installation, designed by [8], is built around a BBC VTR 160L turbocharger that consists of a single-stage, centrifugal compressor with a vaned diffuser, which is mounted on the same rotational axis as the single-stage, axial expander. Expansion requires a pressure ratio across the expander, so first the gas has to be compressed. By mounting the expander on the same axis as the compressor, it can deliver the power to pressurize the incoming gas. To increase the net mechanical power provided at the shaft, the temperature of the working gas is raised by burning fuel in the combustion chamber.

For studies involving compressor surge, the gas turbine installation is mostly used in the configuration shown in Fig. 1, with the dashed connecting line removed. Similar to [2], the mass flows through the compressor and expander are now decoupled; the compressor pressurizes the incoming air which is discharged via the compressor blow-off valve into the atmosphere. This modified configuration offers the following benefits. First, the occurring surge oscillations are assumed to be less harmful for the equipment, since the compressor discharges in a relatively small *plenum volume* compared to the large vessel of the standard gas turbine installation. Second, [2] showed that in this small volume case the steady-state compressor characteristics can be determined up to smaller mass flows. Third, if the compressor and expander mass flows are coupled, the number of steady operating points reduces significantly because a power and mass balance holds between both components [8, 9]. In the studied system, externally supplied compressed air flows via the expander throttle valve into the combustion chamber where natural gas is added and burned. As the compressor and expander mass flows can be varied independently, the modified system can in principle be operated in any desired operating point. However, in this configuration the rotational speed can be varied up to 25,000 [rpm] due to the limited mass flow rate of the externally supplied compressed air.

For higher compressor speeds the gas pressurized by the compressor can supplement the externally supplied compressed air, by using the dashed connecting line and closing the compressor blow-off valve. Because in this configuration, that includes the large vessel, surge is much more powerful and is of lower frequency, no extended surge measurements are possible, otherwise damage to the machine could easily occur. Some characteristic turbocharger data is summarized in Table 1.

Table 1: Parameters of the BBC turbocharger

Part	Parameter	Value	Unit
Impeller	number of blades, Z	20	-
	inlet diam. at casing, D_{t1}	0.106	m
	inlet diam. at hub, D_{h1}	0.054	m
	exit diameter, D_2	0.180	m
	exit width, b_2	0.007	m
	blade inlet angle, β_{1b}	40	deg
Vaned	number of vanes, z	45	-
diffuser	inlet diameter, D_3	0.215	m
	outlet diameter, D_4	0.258	m
	vane inlet angle, α_{2b}	28	deg
System	Plenum volume, V_p	0.0203	m^3
	Duct area, A_1	0.00956	m^2
	Duct length, L_c	1.8	m

2.2 Measurement system
To determine the steady-state performance of the compressor, the compression system is equipped with several temperature probes and pressure transducers, as shown in Fig. 1. Moreover, steady expander and compressor blow-off mass flows can be determined from two instrumented orifices whereas the rotational speed of the impeller is measured with a semi-conductor pulse tachometer. The angular displacement of the stem of the expander throttle and compressor blow-off valve is also registered. This signal is a measure for the opening

area of the valves. As these valves have a linear flow characteristic, the mass flow through the valve is proportional to the valve position [8]. For data-acquisition, a NATIONAL INSTRUMENTS board is plugged in a measurement PC. LABVIEW software controls the data storage on hard disk and real-time process monitoring on the computer screen. This system runs at 200 [Hz] sampling frequency. A second PC equipped with a dSPACE DS1103 control board is used to run (surge) controllers and to gather a subset of the available data at high speeds, because it is set at 1 [kHz] sampling frequency. Compressor transients are observed using measurements of the high-frequency response pressure probe at the compressor outlet, of the compressor blow-off valve's rotation angle sensor, and of the rotational speed transducer. Reliable, transient mass flow measurements are not available.

3 Model

The model to be validated is in the form

$$
\begin{aligned}
\dot{p}_p &= \frac{a_{01}^2}{V_p}(m - m_t) \\
\frac{L_c}{A_1}\dot{m} &= p_{02} - p_p \qquad (1) \\
J\dot{\omega} &= \tau_t - \tau_c,
\end{aligned}
$$

where m is the compressor mass flow, p_{02} is the pressure downstream of the compressor, a_{01} is the inlet stagnation sonic velocity, L_c is the length of compressor and duct, A_1 is the area of the impeller eye (used as reference area), J is the central moment of inertia of the shaft including mounted parts, τ_t is the turbine drive torque and τ_c is the compressor torque. The two first equations of (1) are equivalent to the model of [5]. The model is derived by calculating the mass balance of the plenum volume, integrating the one dimensional Euler equation (the momentum balance) over the length of the exit duct, and calculating the torque balance of the rotating shaft. A detailed derivation of (1) can be found in [3] or [4], and we will here only present some modifications/refinements to the derivation in [3].

3.1 Compressor and turbine torques.
For turbomachines, applied torque equals the change in angular momentum of the fluid:

$$
\tau_c = m(r_2 C_{\theta 2} - r_1 C_{\theta 1}), \qquad (2)
$$

where τ_c is the compressor torque, $r_1 = \frac{D_1}{2}$, $r_2 = \frac{D_2}{2}$ and $C_{\theta 2}$ is the tangential component of the gas velocity C_2. Power delivered to the fluid is

$$
\dot{W}_c = \omega\tau_c = m(U_2 C_{\theta 2} - U_1 C_{\theta 1}) = m\Delta h_0 \qquad (3)
$$

where Δh_0 is the specific enthalpy delivered to the fluid without taking account for losses. Velocity triangles coresponding to (2) and (3) can be found in [4]. A radially vaned impeller is considered with $\beta_{2b} = 90°$, and there is no pre-whirl, that is $\alpha_1 = 90° \Rightarrow C_{\theta 1} = 0$. These assumptions are valid for the compressor of the VTR 160. However, the model can easily be extended to handle both backsweep and pre-whirl. The compressor torque is given by

$$
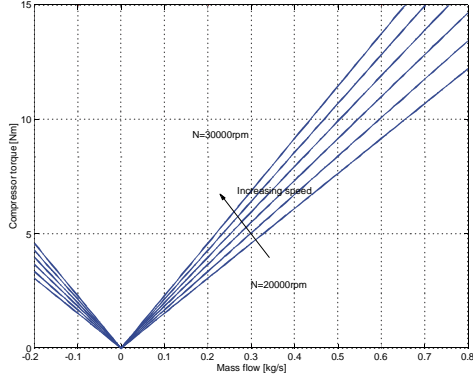\tau_c^+ = mr_2 C_{\theta 2} = mr_2\sigma U_2, \ m > 0, \qquad (4)
$$

Figure 2: Compressor torque

where σ is the slip factor. The torque calculated in (4) is for forward flow. However, the compressor may enter deep surge, and there is need for an expression for the compressor torque at negative mass flow. It will be assumed that the compressor torque of a centrifugal compressor in reversed flow can be calculated by the use of Euler's turbine equation:

$$\tau_c^- = m(r_1 C_{\theta 1} - r_2 C_{\theta 2}) = -mr_2\sigma U_2, \ m < 0. \quad (5)$$

Combination of (4) and (5) gives

$$\tau_c = |m|r_2\sigma U_2. \quad (6)$$

The torque characteristic of the VTR 160 compressor, calculated using (6), is shown in Fig. 2. In [2] a *constant* turbine torque was used for studying the transients of the compressor system. As the turbine torque is dependent on other system states as N, that will vary under transient conditions, this approach will not be used here. The turbine torque is found by dividing turbine power with angular velocity:

$$\tau_t = \frac{P_t}{\omega} = \frac{\eta_m m_{turbine} c_{p,t} \Delta T_{0,turbine}}{2\pi N} \quad (7)$$

where $\Delta T_{0,turbine} = T_{t,in} - T_{t,out}$ is the stagnation temperature drop over the turbine, η_m is the turbine mechanical efficiency, which is usually very high, $\eta_m = 0.99$ being typical, $m_{turbine}$ is the turbine mass flow, $c_{p,t}$ is the turbine specific heat under constant pressure and N is the rotational speed of the shaft.

Notice that the ideal enthalpy Δh_0 defined in equation (3) is independent of mass flow m, and ideally we would have the same energy transfer for all mass flows. However, due to various losses, the energy transfer is not constant, and we will now include this in the analysis. According to [10], the two major losses, expressed as specific enthalpies, are: *1) Incidence losses*, Δh_i and *2) Fluid friction losses*, Δh_f. Other losses such as inlet casing losses, disc friction losses, leakage losses and collector losses do occur, but these will not be considered here. Moreover, the incidence losses and fluid friction losses play an important role in shaping the compressor characteristic and determining the region of stable operation for the compressor. Depending on the mass flow being lower or higher than the design flow, positive or negative stall is said to occur. The velocity of the incoming gas relative to the inducer is denoted W_1. In off-design operation there will be a mismatch between

the *fixed* blade angle β_{1b} and the direction of the flow $\beta_1 = \beta_1(U_1, C_1)$. The angle of incidence is defined by $\beta_i = \beta_{1b} - \beta_1$. As the gas hits the inducer, its velocity instantaneously changes its direction to comply with the constant blade inlet angle β_{1b}. The direction is changed from β_1 to β_{1b}, and the kinetic energy associated with the tangential component $W_{\theta 1}$ of the velocity is lost. Due to continuity, the radial component of the velocity must remain unchanged. The incidence loss can now be expressed as

$$\Delta h_{ii} = \frac{W_{\theta 1}^2}{2} = \frac{1}{2}\left(U_1 - \frac{\cot\beta_{1b} m}{\rho_{01} A_1}\right)^2. \quad (8)$$

The detailed derivation may be found in [3]. The losses in the vaned diffuser can be modeled in a similar manner, and it is assumed that the velocity of the fluid entering the diffuser is instantaneously changed to comply with the fixed diffuser inlet angle α_{2b}. The direction is changed from α_2 to α_{2b}, and the kinetic energy associated with the tangential component C_{3i} of the velocity is lost. That is, the diffuser incidence loss can be expressed as

$$\Delta h_{id} = \frac{C_{3i}^2}{2} = \frac{1}{2}\left(\sigma U_2 - \cot\alpha_{2b} C_{a3}\right)^2. \quad (9)$$

The velocity C_{a3} is calculated by assuming incompressible flow in the vaneless space. According to [1] loss due to friction in the impeller can be calculated as

$$\Delta h_{fi} = f_i \frac{l_i}{D_i}\frac{W_{1b}^2}{2}, \quad (10)$$

where f_i is the impeller friction factor, l_i is the mean impeller channel length and D_i is the impeller mean hydraulic channel diameter. For calculation of the friction factor, we use Haalands explicit formula, [11] :

$$\frac{1}{f_i^{1/2}} = -1.8\log\left(\frac{6.9}{\text{Re}} + \left(\frac{\epsilon/D_i}{3.7}\right)^{1.1}\right). \quad (11)$$

The Reynolds number used is Re $= \frac{U_2 b_2}{\nu}$,where b_2 is the impeller tip width and ν is the kinematic viscosity at the impeller inlet. This was recommended by [7] as being a representative value of the Reynolds number for a centrifugal compressor stage. The mean hydraulic channel diameter D_i is defined as $D_i = \frac{4A_i}{a_i}$ where the cross section area A_i and wetted perimeter a_i are mean values for the passage. For the impeller, the mean hydraulic diameter is set to the average of the inducer inlet hydraulic diameter and the impeller exit hydraulic diameter. Using $W_{1b} = \frac{C_1}{\sin\beta_{1b}}$, we get

$$\Delta h_{fi} = \frac{f_i l_i}{2D_i \rho_1^2 A_1^2 \sin^2\beta_{1b}} m^2 = k_f m^2. \quad (12)$$

The friction loss Δh_{fd} in the diffuser is calculated using the mean hydraulic diameter of the diffuser passages, resulting in an expression similar to (12).

3.2 Pressure rise.
The pressure rise in the compressor is from the stagnation pressure p_{01} at the inlet, to the stagnation pressure p_{02} at the outlet. Generally, this rise in stagnation pressure can be obtained in an isentropic process $1 \rightarrow 2s$
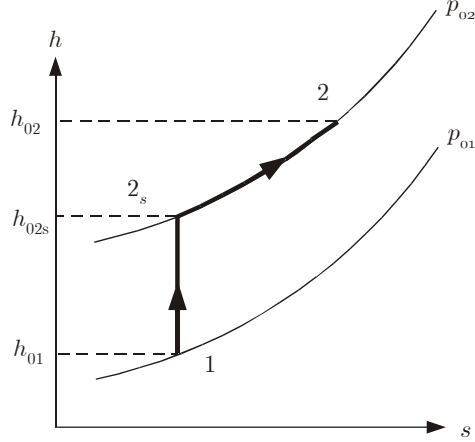
Figure 3: Isentropic / isobaric process in the compressor.

where $p_{02s} = p_{02}$ which involves an increase in the stagnation enthalpy $\Delta h_{0s} = h_{02s} - h_{01}$. The pressure increase in the compressor is not isentropic, and there is an increase in entropy due to incidence losses Δh_i and friction Δh_f. To account for this, the compression from p_{01} to p_{02} is modeled as an isentropic process in series with an isobaric process. For the isentropic process, the entropy differential is $ds = 0$ and the enthalpy differential is $dh = vdp$, while for the isobaric process $dp = 0$ and $dh = Tds$. This results in the following description: First, there is an isentropic process $1 \rightarrow 2s$ which ends in a state with pressure $p_{02s} = p_{02}$ and stagnation enthalpy h_{02s}. Then, there is an isobaric process $2s \rightarrow 2$, which accounts for the entropy increase and ends in a state with pressure p_{02} and stagnation enthalpy h_{02}.

The total process $1 \rightarrow 2$ is illustrated in Fig. 3, and

$$
\begin{aligned}
\Delta h_{02} &= \Delta h_{02s} + \int_{2s}^{2} Tds \qquad (13)\\
&= \Delta h_{02s} + \Delta h_{ii} + \Delta h_{fi} + \Delta h_{id} + \Delta h_{fd}
\end{aligned}
$$

Here Δh_{ii} and Δh_{id} are the incidence losses, Δh_{fi} and Δh_{fd} are the friction losses, and Δh_{02s} is the change in specific stagnation enthalpy that contributes to the acceleration of the gas in the duct. The stagnation pressure ratio is given by the stagnation temperature ratio of the isentropic process $1 \rightarrow 2s$ according to

$$
\frac{p_{02}}{p_{01}} = \left(\frac{T_{02s}}{T_{01}}\right)^{\frac{\kappa}{\kappa-1}} \qquad (14)
$$

An expression for T_{02s}/T_{01} is found from

$$
\frac{T_{02s}}{T_{01}} = \frac{h_{02s}}{h_{01}} = \frac{h_{01} + \Delta h_{02s}}{h_{01}} = 1 + \frac{\Delta h_{02s}}{h_{01}} = 1 + \frac{\Delta h_{02s}}{c_p T_{01}} \qquad (15)
$$

which gives

$$
\Psi_c(m,\omega) = \frac{p_{02}}{p_{01}} = \left(1 + \frac{\Delta h_{0s}}{c_p T_{01}}\right)^{\frac{\kappa}{\kappa-1}}. \qquad (16)
$$

The mass flow m_t through the throttle is modeled as $m_t = k_t\sqrt{p_p - p_{01}}$, where k_t is the throttle gain proportional to throttle opening and p_p is the plenum pressure.

We now have the following dynamic model for the compression system:

$$
\begin{aligned}
\dot{p}_p &= \frac{a_{01}^2}{V_p}(m - k_t\sqrt{p_p - p_{01}})\\
\dot{m} &= \frac{A_1}{L_c}\left(\left(1 + \frac{\Delta h_{02s}}{T_{01}c_p}\right)^{\frac{\kappa}{\kappa-1}} p_{01} - p_p\right) \qquad (17)\\
\dot{\omega} &= \frac{1}{J}\left(\tau_t - \tau_c\right),
\end{aligned}
$$

where (16) has been inserted in (1).

4 Comparison with experimental results

The response of the model (17) was compared to the measured response from the lab in three different classes of experiments. First, the calculated compressor characteristic in equation (16) was compared to the measured characteristic for three different rotational speeds. Then set point changes using both the blow off valve and the fuel supply were conducted and compared to simulations. Finally the compressor was driven into surge and the measured surge oscillation was compared to a corresponding simulation.

4.1 Compressor characteristic
In these experiments, the compressor characteristic was measured for three speed lines ($N = 18000$[rpm], $N = 21000$[rpm] and $N = 23000$[rpm]). For each speed, the measurements started at high mass flow, and the flow was gradually reduced until surge was encountered. The measurements are shown with 'x'-es interconnected with solid lines in Fig. 4. A calculated compressor map is shown with solid lines in Fig. 4. These speed lines were calculated using (16). For negative flows, the compressor characteristic was calculated using

$$
\Psi_c(m,\omega) = c_n m^2 + \psi_{c0}(\omega), m < 0 \qquad (18)
$$

selecting a suitable value for c_n, and calculating $\psi_{c0}(\omega)$ by inserting $m = 0$ in (16). As can be seen, experiment and theory match very well in the neighborhood of the surge line, marked with the shaded area in Fig. 4. The dashed line represents the line between the maxima of the calculated speed lines, and it is almost indistinguishable from the line connecting the endpoint of the measured speed lines, that is the surge line. For higher mass flows there is an increasing deviation between theory and measurement. The reason for this might be due to the incidence loss model (8) and (9) only being valid in a limited range around the design flow. Other mechanisms responsible for the steep slope of the measured characteristic could be losses not taken account for (leakage, disc friction, etc.) or choking. This is currently being studied more closely. However, it should be emphasized that measurement and calculation of the compressor pressure rise, is in agreement within 2% up to about 40% above the surge flow.

4.2 Set-point changes
Two different types of set point changes were performed. First using the blow off valve, and then using the fuel valve. The transient measurements were then compared to simulations. Because of difficulties in measuring the turbine exit temperature $T_{t,out}$, the temperature drop over the turbine $\Delta T_{0,turbine}$ was calculated
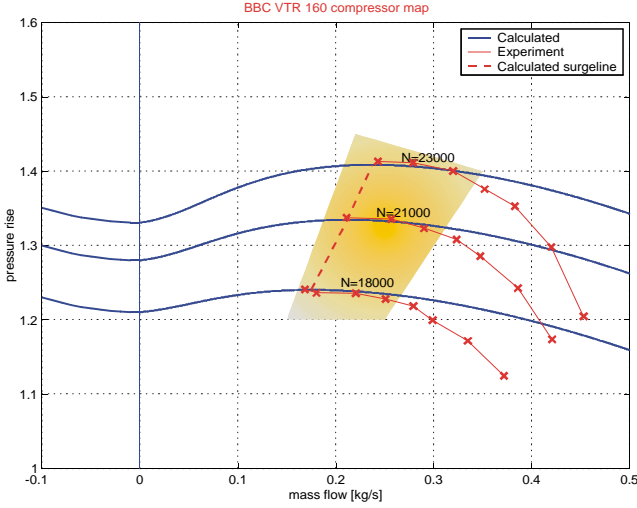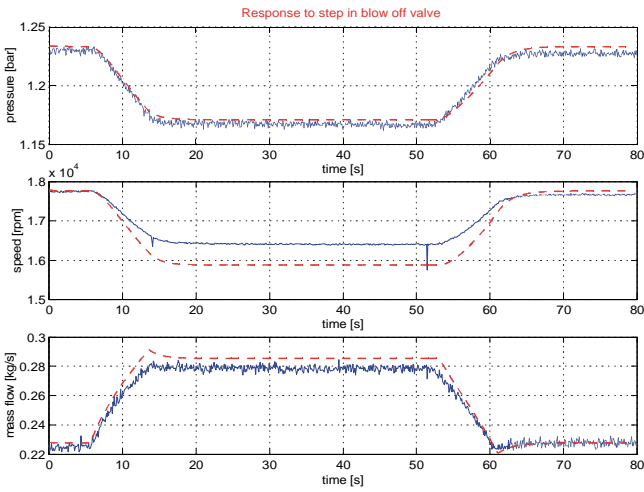
Figure 4: Compressor characteristic

Figure 6: Changing the set point using the fuel valve

Figure 5: Changing the set point using the blow off valve.

from the compressor torque τ_c at constant rotational speed.

Blow off valve: In this experiment the blow off valve was used to change the set point. The measurements and corresponding simulations are shown in Fig. 5. At $t = 5.7$s, the blow off valve position was changed from $Y_b = 3.485$V to $Y_b = 4.395$V, and back again at $t = 52$s. From the mass flow measurements it was found that this corresponds to a step in k_t from 0.00015 to 0.00022. The blow off valve is modeled as a step and a rate limiter. The valve is rather slow, with a maximum slew rate of 0.11V/s. As can be seen from Fig. 5, the simulation and measurement are in good agreement, except for the steady state of the rotational speed. This is attributed in part to the deviation in the compressor characteristic and in part to the difficulties in calculating the drive torque from measured turbine temperature drop. The spikes seen in the speed measurments in Fig. 5, and also Fig. 6, are due to a grounding problem in the buttons commanding the opening of the fuel- and blow off valves.
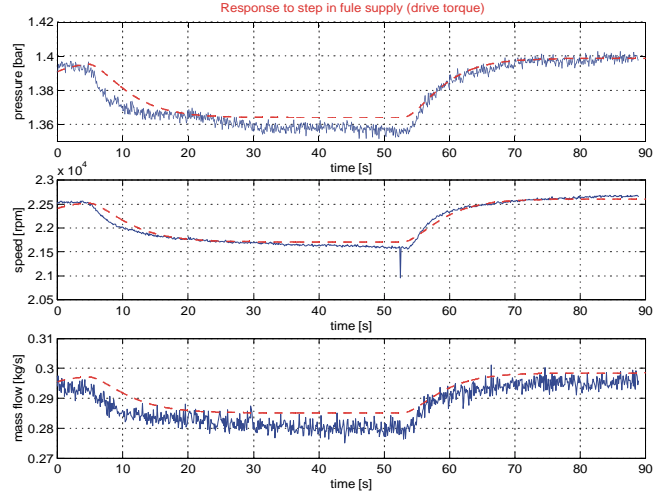
Fuel valve/drive torque: In this experiment the fuel valve was used to change the set point. This is equivalent to manipulating the drive torque. The measurements and corresponding simulations are shown in Fig. 6. At $t = 4.1$s, the fuel valve position was changed from $Y_g = 2.06$V to $Y_b = 1.68$V, and to $Y_b = 2.134$V at $t = 48.6$s. This corresponds to a step in turbine temperature drop of -3.06K at $t = 4.1$s and 3.30K at $t = 48.6$s. The temperature drops were computed from the calculated compressor torque. From the mass flow measurements it was found that k_t=0.00015. The turbine responds quite slow to a change in fuel supply, and a time constant of 8s between the temperature change ΔT_t and the drive torque τ_d was used to take this into account. As shown in Fig. 6, the measurement and simulation for this kind of set point change are in good agreement.

4.3 Surge experiment

In this experiment, the compressor was initially operating close to the surge line, and then driven into surge using the blow off valve. During the surge cycles, pressure and rotational speed were logged using the dSPACE DS1103 control board. In the upper part of Fig. 7, the pressure transient when the compressor enters surge is shown and compared to a simulation of the same situation (dashed lines). A more detailed comparison is shown in the lower plot of Fig. 7, which is a zoomed-in version of the upper plot. There is some deviation between the measured surge frequency (20 Hz), and the simulated surge frequency (23 Hz). This is most likely due to the mismatch between the slopes of the real and calculated compressor characteristics, as the surge frequency is dependent on this slope, [12]. When the compressor is operating in surge, the rotational velocity of the shaft is also oscillating. The amplitude of this oscillation is dependent on the size of the plenum volume V_p. As we here operate with a relatively small volume, it is to be expected that these oscillations are of a low amplitude. Simulations show that at a nominal speed of $N = 20000$[rpm], the amplitude of the surge induced speed variations is 40[rpm]. The measured oscillations in rotational speed are of such a small amplitude, that they are not distinguishable from the noise in the measured signal. However, the power spectrum of the measured speed, in Fig. 9, shows that after the compressor
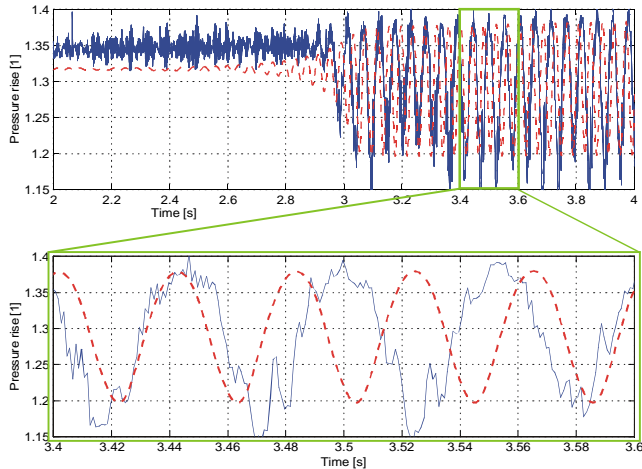
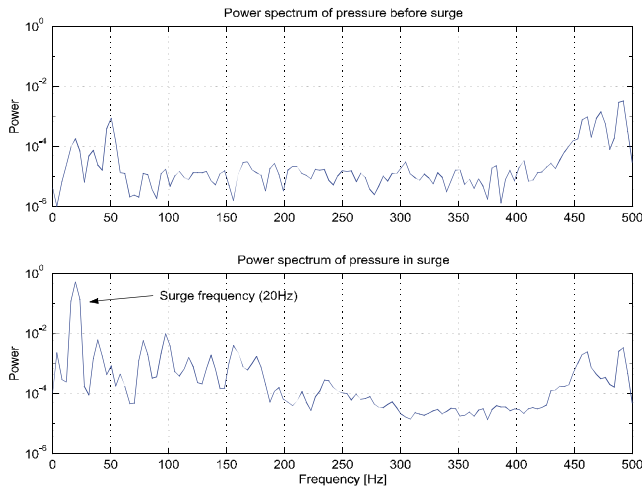**Figure 7:** Comparison of surge experiment and simulation

Figure 8: Power spectrum of pressure measurement

Figure 9: Power spectrum of speed measurement

has entered surge (lower part of Fig. 9) the speed signal has a strong component at around 20Hz, the surge frequency, that was not present before the surge event. This is also seen in the power spectrum of the pressure signal in Fig. 8.

5 Concluding remarks and further work

Comparison of simulations of a compression system model and measurements from a gas turbine installation show that the model predicts the transients, both stable and unstable, well. Transients in both pressure, mass flow and rotational speed were compared, and both stable set point changes and surge were covered.

Further work includes improved modeling of the compressor characteristic by improving the incidence loss model, or taking account for other losses. Also in order to study the variations in rotational speed during surge more closely, it would be interesting to perform experiments with a larger plenum volume, as we expect the variations to be larger and therefore easier to verify.
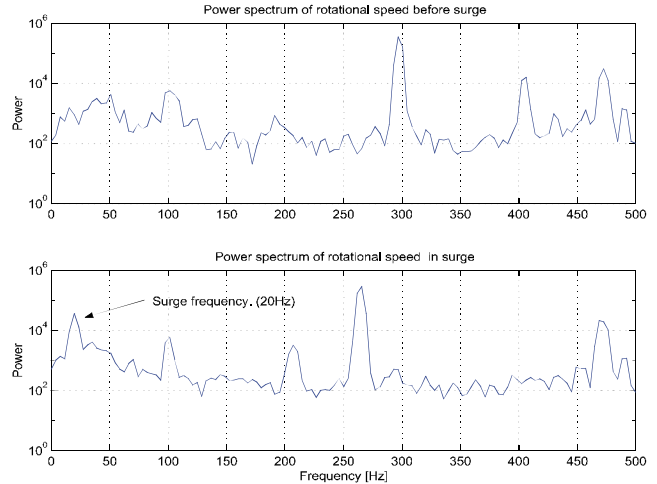
6 Acknowledgments

References

[1]   T.B. Ferguson.   *The centrifugal compressor stage.* Butterworths, London, 1963.

[2]   D.A. Fink, N.A. Cumpsty, and E.M. Greitzer. Surge dynamics in a free-spool centrifugal compressor system. *Journal of Turbomachinery*, 114:321–332, 1992.

[3]   J.T. Gravdahl and O. Egeland. Centrifugal compressor surge and speed control. *IEEE Transactions on Control Systems Technology*, 7(5), 1999.

[4]   J.T. Gravdahl and O. Egeland. *Compressor surge and rotating stall: modeling and control.* Advances in Industrial Control. Springer-Verlag, London, 1999.

[5]   E.M. Greitzer. Surge and Rotating stall in axial flow compressors, Part I: Theoretical compression system model. *Journal of Engineering for Power*, 98:190–198, 1976.

[6]   K.E. Hansen, P. Jørgensen, and P.S. Larsen. Experimental and theoretical study of surge in a small centrifugal compressor. *J. of Fluids Engineering*, 103:391–394, 1981.

[7]   R.A Strub, L. Bonciani, C.J. Borer, M.V. Casey, S.L Cole, B.B. Cook, J. Kotzur, H. Simon, and M.A. Strite. Influence of the reynolds number on the performance of centrifugal compressors. *Jornal of turbomachinery*, 109, 541–444 1987.

[8]   H. van Essen. Design of a laboratory gas turbine installation. Technical Report WOC-WET 95.012, Institute for Continuing Education (IVO), Fac. of Mecanical Engineering, Eindhoven University of Technology, March 1995.

[9]   H. van Essen. *Modelling and Model Based Control of Turbomachinery.* PhD thesis, Fac. of Mechanical Engineering, Eindhoven University of Technlogy, November 1998.

[10]   N. Watson and M.S. Janota. *Turbocharging the internal combustion engine.* MacMillan, 1982.

[11]   F.M. White. *Fluid mechanics.* McGraw-Hill, New York, 2nd edition, 1986.

[12]   F. Willems. Modeling and bounded feedback stabilization of centrifugal compressor surge. Ph.D. Thesis, Fac. of Mechanical Engineering, Eindhoven University of Technology, 2000.